Using Delta Differential One-Way Range to Determine Highly Elliptical Earth Orbits

Raymond B. Frauenholz*
Jet Propulsion Laboratory, California Institute of Technology, Pasadena, California

Acquisition strategies for delta differential one-way range measurements are designed for determining highly elliptical Earth orbits. The mission orbit for the U.S. Charged Composition Explorer spacecraft of the international Active Magnetospheric Particle Tracer Explorers serves to illustrate these acquisition techniques. The study assumes intercontinental baselines formed by Deep Space Network antennas at Goldstone, Canberra, and Madrid. The best performing strategy employs data spanning baseline view periods covering both inbound and outbound legs near the same orbit periapse. Rapidly changing viewing geometry yields both angular position and velocity information but frequently imposes the need for a different reference quasar for each observation. Although limited by an S-band transponder and a small bandwidth, the addition of delta differential one-way range to coherent Doppler and range improves apogee position accuracy by more than an order of magnitude. The measurement noise, highly dependent on acquisition geometry, varies several orders of magnitude across the baseline view periods primarily due to parallax. Careful selection of observation times minimizes the geometric influence on data noise. Additional measurement accuracy improvements, possible with dual frequency calibration, increased spanned bandwidth, and water vapor radiometry, are presented for comparison. Quasar position uncertainties then dominate the measurement noise.

Introduction

FOR many years both Earth-orbiting and interplanetary spacecraft navigation has successfully relied on conventional radio metric Doppler and range measurements acquired by a worldwide network of ground stations. These techniques, while effective, frequently require either numerous or long data acquisition periods to achieve the desired navigation accuracies. As the number of missions increase and navigation accuracies become more demanding, antenna requirements often exceed capacity. The recent development and application of Very Long Baseline Interferometry (VLBI) technology serves not only to improve navigation accuracies, but also to reduce antenna support requirements.

The VLBI technique employs two widely separated ground stations to simultaneously receive a signal broadcast by the spacecraft.[1,2] Cross correlation of the received signals provides a precise measure of differential time delay for wide bandwidth signals and rate of change in time delay for narrow bandwidth signals. By also knowing the baseline between the two stations, these delays directly determine single components of instantaneous spacecraft angular position or velocity. Simultaneous measurements from two nonparallel, and preferably orthogonal, baselines combine to determine the total angular position or velocity.

The differential measurement is insensitive to unmodeled spacecraft dynamics, a common problem with single station tracking. Cancellation of common downlink errors improves the measurement accuracy. The effects of a relatively unstable spacecraft frequency reference cancel, and the one-way signal propagation greatly simplifies both charged particle and station electronics delay calibration error sources. In addition to eliminating the need for an uplink, the VLBI technique significantly reduces antenna support requirements, with a single observation requiring only 5–10 min. The wideband VLBI measurement is differential one-way range (DOR); the narrow bandwidth form, differential one-way Doppler (DOD).

Received Aug. 30, 1985; revision received March 24, 1986.

*Member of Technical Staff. Member AIAA.

Two independent VLBI measurements are formed by alternately listening to the spacecraft and to an angularly nearby extra-galactic radio source (quasar) of known direction. Differencing the two VLBI measurements forms a delta VLBI (ΔVLBI) observable. Common ground and spacecraft error sources cancel and reduce effects of transmission media, timing, polar motion, and station location uncertainties. The degree of error reduction depends primarily on spacecraft-quasar angular separation. The wide bandwidth form of ΔVLBI is delta differential one-way range (ΔDOR); the narrow bandwidth measurement is a delta differential one-way Doppler (ΔDOD).

This paper examines the potential of ΔDOR measurements for determining Highly Elliptical Orbits of Earth satellites. These HEO-class orbits are characterized by large eccentricities: $e \geq 0.75$. The mission orbit of the Charged Composition Explorer (CCE) spacecraft of the Active Magnetospheric Particle Tracer Explorers (AMPTE) mission serves to illustrate data acquisition strategies.

A series of Voyager demonstrations[3,4] first established the feasibility of using ΔDOR for interplanetary navigation. This technique is now an effective operational strategy.[5,6] Predictions of geosynchronous orbit determination performance based on theoretical studies[7] have since been successfully demonstrated for the Air Force DSCS II satellite.[8] The Galileo mission requires ΔDOR to satisfy orbit accuracy requirements for Jupiter's approach.[9]

The ΔDOR technique initially was studied for an HEO-class spacecraft using the AMPTE Ion Release Module (IRM)[10] and Deep Space Network (DSN) antennas at Goldstone, Canberra, and Madrid. The study concludes optimum performance results using baseline view periods covering both inbound and outbound legs near the same orbit periapse. Observations near the beginning, middle, and end of each view period, providing six measurements over intervals of maximum rates of change in true anomaly, permit rapid determination of both angular position and velocity. Combining ΔDOR with coherent Doppler and range improves IRM orbit determination accuracy an order of magnitude. Orbit accuracy depends on ΔDOR measurement noise, a strong function of the viewing geometry. The IRM study assumed quasar availability and an optimistic constant 15-cm data noise for all measurements without considering geometric influences.

This paper builds upon IRM study results by developing ΔDOR acquisition strategies constrained by realistic spacecraft-quasar geometry. A theoretical model[11] predicts data noise variations with four key parameters: 1) spacecraft and quasar viewing elevations; 2) spacecraft-quasar separation angles; 3) times between spacecraft and quasar data scans; and 4) duration of each data scan. The primary objective is to develop strategies yielding minimum data noise for each observation. Predicting orbit accuracy for a set of minimum noise measurements is a secondary objective.

The CCE carries a NASA standard near-Earth S-band transponder with a signal bandwidth of only 6.8 MHz. This design limits the ΔDOR data quality by preventing dual frequency calibration capable of virtually eliminating the effects of ionosphere modeling errors. Orbit accuracy predictions with and without dual frequency calibration and a wider bandwidth transponder are evaluated for comparison.

Observable Characteristics

Received Spacecraft Signal

The S-band carrier signal transmitted by the CCE is phase modulated by a 429-kHz sinusoidal subcarrier. Brief tests demonstrated the ±8th harmonics of the subcarrier have sufficient signal strength for acquisition, resulting in a maximum effective spanned bandwidth of 6.864 MHz. The predicted power received at the station, estimated from link analysis,[12] is a very strong −156 dBm (2.5×10^{-16}W).

Ambiguity Resolution

Measuring the phase of the received signal determines only the fractional part of a cycle. The integer part is ambiguous, but needed to form the ΔDOR observable. Resolving this ambiguity requires sufficiently accurate predictions of the quasar delay and spacecraft DOR observable. The differential delay requires an accuracy of one-half cycle at the spanned bandwidth. For the CCE, the bandwidth between adjacent harmonics of the subcarrier is 429 kHz; the time delay for one integer cycle is 1/858 kHz, or 1166 nsec. Forming the observable, using this bandwidth, requires an orbit prediction accuracy allowing determination of the differential one-way range to better than half this amount.

Geometric considerations permit easy estimation of the required orbit accuracy. First determined is the change in spacecraft position corresponding to a change in differential one-way range for one-half cycle (583 nsec). For long baselines, the corresponding orbit position uncertainty varies between 400 and 900 m, depending on the spacecraft altitude during data acquisition ($3\lesssim Re\lesssim 7$). Such orbit accuracy is achievable using coherent Doppler and range.

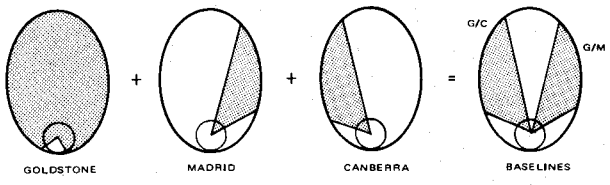

Fig. 1 DSN view periods of AMPTE/CCE for orbit 315, 10 March 1985 (see Table 2 for orbit data).

Data Acquisition Strategy

Baseline View Periods

The IRM study[11] established that six ΔDOR measurements spanning two different baseline view periods covering inbound and outbound legs near the same orbit periapse provide the best results. A CCE survey during March 1985 revealed many DSN baseline view periods, but only two orbits contain a pair. Mission orbits 315 and 341 (March 10 and 27) offer Goldstone/Madrid (G/M) and Goldstone/Canberra (G/C) baseline view periods. Figure 1 shows these baseline view periods for orbit 315 in an orbit-relative frame. Note that Goldstone views the spacecraft for most of the orbit while the inbound and outbound legs are covered by the other two complexes.

With an orbital period of 15:40 (see Table 2), similar viewing geometry recurs only every 26 orbits, or 17 days. A slightly larger period of 16 h provides a much more frequent repetition every two days, or three orbit periods. However, without an orbit period adjustment capability, ΔDOR acquisition by two baselines in a single orbit remains limited by the 17-day repeat cycle. The orbit determination performance of this less frequent viewing cycle is studied to develop an understanding of modeling uncertainty propagation. The presence of prominent modeling errors invites a more frequent acquisition interval and demonstrates the value of an on-board maneuver system.

Figures 2a and 2b present the viewing elevations and the topocentric right ascension and declination for the G/M and G/C baselines. Rapid and nonlinear angular changes occur during these view periods. Viewing parallax of the G/M baseline, primarily in right ascension, reflects the difference between station longitudes. Observations acquired by this east-west baseline provide in-plane angular position information for the near-equatorial orbit. Parallax in both right ascen-

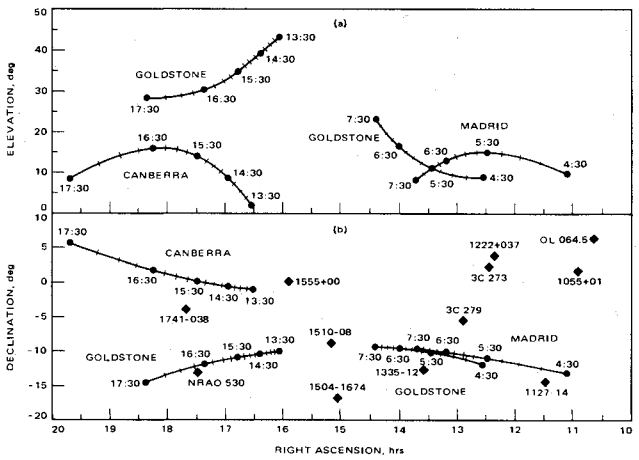

Fig. 2 Spacecraft elevation, right ascension, and declination for the G/M and G/C baselines: a) elevation; b) declination.

Table 1 Quasar one-sigma position uncertainties and signal strength at S-band

G/M baseline					G/C baseline				
Quasar		Correlated flux den	Pos uncert[b] (nrad)		Quasar		Correlated flux den	Pos uncert (nrad)	
No.	Name	(Jansky[a])	RA	DEC	No.	Name	(Jansky)	RA	DEC
1	1127-14	1.50	14	16	4	1555+00	0.50	3	10
2	3C 279	3.70	3	9	5	NRAO 530	1.40	3	10
3	1335-12	1.10	3	10	6	1741-038	0.15	3	8

[a] 1 Jansky = 10^{-23}erg/cm^2/s/Hz. [b] One-sigma uncertainties relative to 1950 equinox.

Table 2 Assumptions and ΔDOR noise contributors

Error sources	Assumptions
1) Zenith troposphere errors 6 cm systematic model 2 cm inhomogeneity	Spacecraft in highly elliptical Earth orbit 1100 km × 8*Re* altitude 5 deg equatorial inclination 15:40 orbital period
2) Oscillator errors short-term instability in station clocks, $\Delta f/f = 10^{-14}$ s/s long-term frequency offset in station clocks, $\sigma_f/f = 10^{-13}$ s/s (assumes calibration)	All observations are S-band $f = 2.271$ GHz Predicted received signal strength -156 dBm $= 2.5 \times 10^{-16}$ W (8th harmonic)
3) Quasar position uncertainty random errors, see Table 1 100 nrad systematic	Station recording channel bandwidth 250 kHz for Blk I
4) Baseline uncertainty 20 cm each component for DSN baselines	Station system temperatures 35K (64-m antenna)
5) Timing (UT1) 30 cm	Effective spanned bandwidth 6.864 Mhz
6) Polar motion 30 cm in each component	Sun-Earth-quasar angular separation >20 deg
7) Quasar system noise correlated flux density at S-band (see Table 1)	Spacecraft-station-quasar angular separation <20 deg
8) Spacecraft system noise predicted received power 2.5×10^{-16} W	Spacecraft/quasar scan durations selected for adequate SNR
9) Phase dispersion 1 deg for DSN Mark IVA stations	Time between spacecraft and quasar scans selected to minimize total noise
10) Ionosphere (assumes Faraday rotation) 20 cm peak 40 cm bias 40 cm spatial fluctuation	

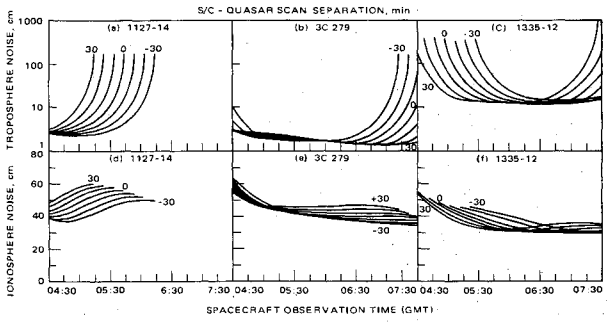

Fig. 3 Troposphere and ionosphere contributions to ΔDOR data noise vs S/C-quasar scan separation for the G/M baseline.

sion and declination for the G/C baseline reflects differences in the station latitudes and longitudes. Data acquired by this baseline contain both in-plane and cross-track angular position information. Observations from both baselines, although not simultaneous nor orthogonal, provide estimates of the total angular position.

Quasar Selection

The quasar population shown in Fig. 2b includes three radio sources near each baseline view period. Table 1 lists these quasars in order of increasing right ascension, the direction of spacecraft motion and order of acquisition. The International Astronomical Union (IAU) designates quasars by inertial position, defined as hhmm±dd for hours and minutes of right ascension, and degrees of declination with the appropriate sign. Quasars are also known by their common name. The correlated flux densities and position uncertainties have been derived from intercontinental baselines at S-band frequency.[13] The DSN Block I VLBI system currently detects radio sources with signal strengths of at least 0.2 Jansky. Most quasars in the navigation catalog[13] have a signal strength between 0.2–1.0 Jansky, so all sources listed in Table 1, except 1741-038, are exceptionally strong.

The six ΔDOR observations acquired using these quasars vary in effectiveness, depending on the measurement noise and the true anomaly change between observations. Understanding how operational considerations influence these factors is also important. Initially, contributors to measurement errors are identified, followed by a description of desirable operational techniques to minimize geometric influences on data noise. System hardware improvements allowing further noise reduction are then discussed.

Measurement Errors

A theoretical error model[11] predicts total ΔDOR measurement noise in terms of ten major contributors. The model formulation is not repeated here; instead the contributors are identified and their influence discussed. There are two types of error sources: those influenced primarily by acquisition geometry, and those resulting from ground system and flight hardware design. Table 2 lists each error source and summarizes the modeling assumptions.

The data noise sensitivity to viewing geometry is assessed by varying the spacecraft observation epoch across each view period, assuming use of each quasar in turn. The goal is to separate each observation by the maximum true anomaly while maintaining a favorably low data noise. However, the pursuit of epochs yielding minimum data noise must be balanced against several operational factors. The stations need sufficient time to acquire each measurement, including scan-

ning each source and antenna pointing changes between each scan.

Error sources affected most by geometric changes are the baseline, troposphere, and ionosphere. Other error sources are primarily functions of ground system and spacecraft hardware design. Initially, the strategy design seeks to diminish geometric influences on data noise, followed by predicted reduction with system improvements.

Troposphere and Ionosphere Influence

The troposphere contribution to data noise results from systematic calibration errors and horizontal inhomogeneities, which both scaled inversely with source viewing elevation.[11] For interplanetary applications, where viewing geometry slowly varies, minimum troposphere influence results using the nearest quasar and observing the spacecraft near view period zenith. Nearly complete error cancellation results when forming the ΔDOR measurement. This strategy is often repeatable over many months using the same quasar and similar viewing geometry.

Viewing geometry of HEO spacecraft changes rapidly during a single baseline view period. The combination of a nearby spacecraft and the long baseline can introduce viewing parallax (Fig. 2) that prevents the usual degree of error cancellation when forming the spacecraft DOR observation. As a result, data noise may vary several orders of magnitude during the view period. The noise reduces by minimizing the spacecraft-quasar angular separation, controlled by the spacecraft acquisition epoch and the separation time between spacecraft and quasar data scans.

The troposphere error contribution reduces further using a water vapor radiometer (WVR). Pointing this ground instrument along the local zenith reduces the systematic error, while pointing along the station line of sight also reduces the random portion. Although not yet operational, a prototype WVR system suggests both systematic and random errors reduce to the 1-cm level, as compared to the larger uncalibrated values listed in Table 2. However, as will be evident later, this systematic improvement contributes little to overall data noise reduction unless also accompanied by dual frequency calibration and an increased spanned bandwidth.

The uncertainties in ionosphere also contribute significantly to ΔDOR noise through spatial and temporal fluctuations and system calibration errors. Like the troposphere, ionosphere errors scale directly with spacecraft-quasar angular separation and inversely with station elevation.[11] After optimizing these angles by epoch selection, dual frequency calibration provides the most effective means of reducing ionospheric contributions.

Troposphere and Ionosphere Data Noise

Figures 3 and 4 present the troposphere and ionosphere contributions to data noise for the three nearest quasars during each baseline view period. The noise is evaluated for a range of representative separation times between the spacecraft and quasar scans. These data show that measurement noise depends primarily on the spacecraft observation epoch and much less on time spacing from the quasar scan. As a result, a common quasar scan 10 min prior to the spacecraft scan time was selected for all quasar observations in this study.

Comparison of data in Figs. 3 and 4 show that the ionosphere contribution usually exceeds that of the troposphere. Once the geometric influences have been minimized, the ionosphere error reduces with dual frequency calibration, whereas the troposphere error relies on WVR calibration. The benefits of these system improvements are reflected later by comparing total data noise.

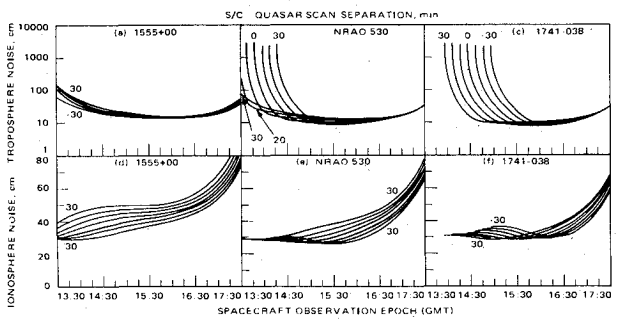

Fig. 4 Troposphere and ionosphere contributions to ΔDOR data noise vs S/C-quasar scan separation for the G/C baseline.

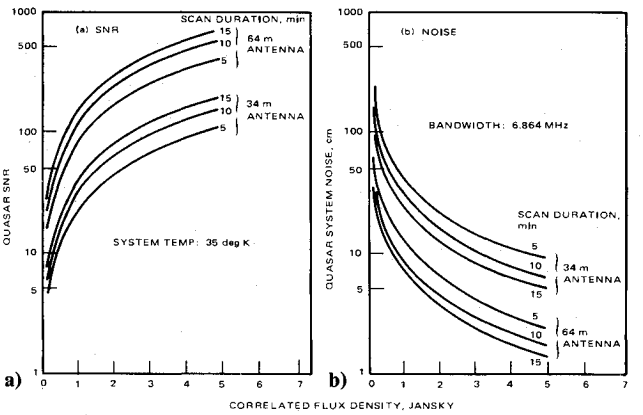

Fig. 5 Quasar signal to noise ratio and system noise: a) variation in quasar SNR, b) quasar system noise.

Table 3 Total ΔDOR measurement noise

Obs. no.	Baseline	Quasar name	Epoch (GMT)	Total ΔDOR data noise (cm) Case I	Case II	Case III	Case IV
1	G/M	1127-14	04:45	62	48	30	18
2	G/M	1335-12	05:45	57	42	21	12
3	G/M	1335-12	06:45	49	41	17	12
4	G/C	NRAO 530	14:30	50	45	24	18
5	G/C	NRAO 530	15:30	48	41	18	15
6	G/C	NRAO 530	16:30	55	42	19	14

Case I: nominal, consistent with Table 2 information
Case II: nominal with S/X calibration
Case III: nominal with S/X calibration and 38 MHz bandwidth
Case IV: nominal with S/X calibration, 38 MHz bandwidth, and WVR calibration

Quasar Position

Since estimating achievable orbit accuracy using differential measurements is a goal of this study, the quasar coordinates are assumed to be suitably accurate for navigation and are based on the same modeling assumptions used in orbit determination.[13] Table 1 lists quasar position uncertainties consistent with these assumptions.

The noise contribution due to quasar position uncertainty varies between 7–14 cm, increasing with the angle between the baseline and the line of sight to the quasar. An error of this magnitude emerges as a dominant contributor to total data noise after realizing the benefits of dual frequency and WVR calibration and increased spanned bandwidth. Further data noise reduction requires improved quasar coordinates.

Phase Dispersion

A nonlinear ratio of phase to frequency response at the receiving stations causes spacecraft and quasar signals to see different phase delays. For the DSN Mark IVA system, this error is on the order of 1 deg/channel for each station. The phase dispersion error scales inversely with spanned bandwidth, having a large value of 34 cm for the CCE. This influence reduces to only 7 cm by increasing the bandwidth from 6.864 to 38 MHz. This larger bandwidth represents a realistic choice since Galileo has selected a 38 MHz wideband transponder dedicated to ΔDOR acquisition. Histograms ranking individual noise contributors show how increasing the spanned bandwidth dramatically reduces total data noise.

System Thermal Noise

System thermal noise varies with radio source signal strength, gains and system temperatures of receiving stations, and spanned bandwidth of the received signal.[11] Noise influences reduce by increasing the signal to noise ratio (SNR) of both spacecraft and quasar signals.

The spacecraft SNR varies directly with received power level. Link analysis[12] indicates a more than ample signal of -156 dBm, or 2.5×10^{-16} W. System noise is negligible for this powerful signal.

Experience with the Voyager indicates that a quasar SNR of at least 10 is desirable. Figure 5a shows the variation in quasar SNR with correlated flux density, antenna aperture, and scan duration. Use of a 64-m antenna provides an SNR exceeding 10 for all considered flux densities and scan durations. However, to obtain this SNR with a 34-m antenna requires flux densities greater than 0.5 Jansky and scan durations of at least 5 min.

Significant quasar system noise results using the 34-m antenna due to limited bandwidth are indicated in Fig. 5b. Even use of a 64-m antenna requires a quasar with a flux density exceeding 0.5 Jansky to reduce noise to the 10–20-cm level, making necessary scan durations of at least 10 min to achieve this performance.

Angular rates of an HEO spacecraft often present problems when tracking near periapse, although CCE rates are well within the 0.25 deg/s maximum rate capability of 64-m antennas. Therefore, this study uses the 64-m antenna throughout.

Use of dual frequency calibration modestly increases the system noise; increasing the spanned bandwidth to 38 MHz virtually eliminates this error source.

Oscillator

An offset in station clock frequencies and station clock instability contribute to the oscillator error. Random short term effects of clock instability are negligible using high quality hydrogen maser timing systems. The larger systematic effects of frequency offset result from long term rate differences between the two station clocks, reduced by minimizing the timed between quasar and spacecraft scans. Additional improvement is possible by estimating the clock offset from quasar scans both prior to and after the spacecraft scan. However, for HEO applications, care must be taken to assure that this strategy does not increase the influence of other error contributors strongly influenced by rapidly changing viewing geometry.

Baseline, Timing (UT1), and Polar Motion

Uncertainties in the baseline, timing, and polar motion also contribute to ΔDOR measurement noise. Individual station location uncertainties result in baseline magnitude and orientation errors, whereas timing and polar motion modeling uncertainties induce only orientation errors. Recent use of VLBI for navigation has improved the absolute station location uncertainties to 2 m per component, whereas each component of the interstation baseline is known to about 20 cm. Baseline orientation errors result from polar motion and timing uncertainties of 30 cm.

Minimizing the spacecraft-quasar angular separation reduces the collective effect of these error sources on data noise to the 2–5-cm level. Noise of this magnitude emerges as a major contributor once data calibrations reduce the total noise to the 15-cm level.

Total Measurement Noise

Figures 6a and 6b present total ΔDOR measurement noise evaluated across each baseline view period relative to each nearby quasar. These data dictate quasar selection based on total measurement noise. In addition to the assumptions listed in Table 2, epoch selection is constrained so that 1) the quasar is always acquired 10 min prior to the spacecraft; 2) all quasar scans are 10 min; and 3) all spacecraft scans are 5 min.

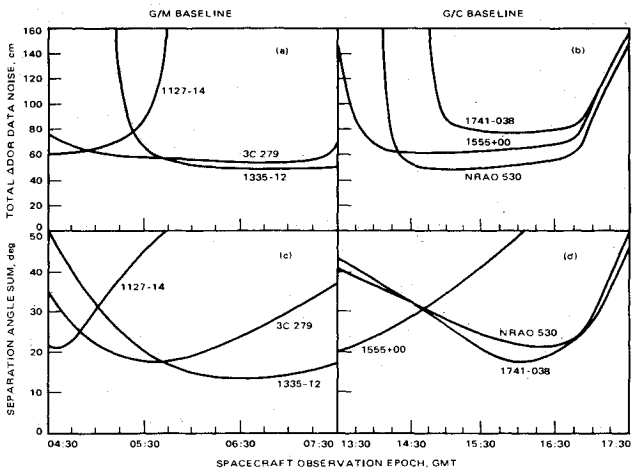

Fig. 6 Total ΔDOR data noise and separation angles for each quasar G/M baseline: a) and c); G/C baseline: b) and d) (separation angle is the sum from each station).

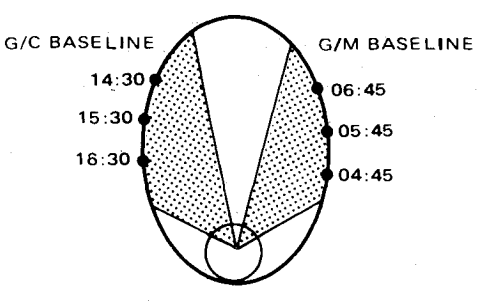

Fig. 7 Orbit position of ΔDOR observation epochs: orbit 315, 10 March 1985.

Table 4 Navigation system error model

Error sources	One-sigma uncertainty
Geopotential field	50% of SAO-APL 8×8 model difference
Earth GM	$GM \times 10^{-8}$
Drag coefficient	100% of nominal coefficient
Solar pressure	10% of nominal reflectivity
Solar flux	30% of nominal 10.7 cm flux
Tropospheric refraction	
for Doppler/range	10% of nominal refraction
for ΔDOR	included in data noise[a]
Station timing	0.1 msec
Station location	
for Doppler/range	
local X and Y	5 m
local Z	15 m
for ΔDOR	included in data noise[a]
Coherent Doppler	
noise	2 cm/s
sample rate	1 sample/min
Coherent range (18 component)	
noise	3 m (deweighted to 100 m for covariance analysis)
bias	15 m
sample rate	1 sample/3 min
ΔDOR noise	a function of specific viewing geometry at acquisition epoch[b]

[a]See Table 2. [b]See Table 3.

Figure 6a indicates minimum noise for data acquired by the G/M baseline results using quasar 1127-14 early in the view period, and quasar 1335-12 subsequently. Selection of quasar 1127-14 at 04:45, and quasar 1335-12 at 05:45 and 06:45 GMT, provides a good balance between minimum data noise and maximum true anomaly change across the view period. A similar process for the G/C baseline results in selection of quasar NRAO 530 during the entire view period, as shown in Fig. 6b. Figure 7 shows the orbit-relative relationship of the six observation epochs to the baseline view periods.

Total noise variation across each baseline view period closely follows the spacecraft quasar angular separation. Because of significant viewing parallax, the sum of the separation angles from each station provides a convenient way to characterize this geometry. Figures 6c and 6d present the total angles for each quasar viewed by each baseline. The minimum angular sum provides a good indicator for both quasar selection and minimum data noise for the G/M baseline but offers misleading information for the G/C baseline. One should select each quasar and spacecraft observation epoch based on measurement noise rather than on geometric information. However, data noise and geometric data should support each other, as they do here.

Table 3 summarizes the data noise improvement as the benefits of dual frequency calibration, increased spanned bandwidth, and WVR calibration are incrementally included in the data strategy. The magnitudes of individual noise contributors for each of these four cases are compared in the histograms of Fig. 8. By including all systematic improvements, as in case IV, the data noise reduces to about one-fourth the nominal value (case I). The achievable orbit accuracies for these two extremes are then compared with the capabilities of coherent Doppler and range.

Predicted Orbit Accuracy

Doppler and Range

Establishing the navigation capability using coherent Doppler and range provides a meaningful reference for comparison to ΔDOR performance. This reference strategy easily satisfies the CCE orbit accuracy requirements, dictated primarily by antenna pointing predictions rather than by science objectives.

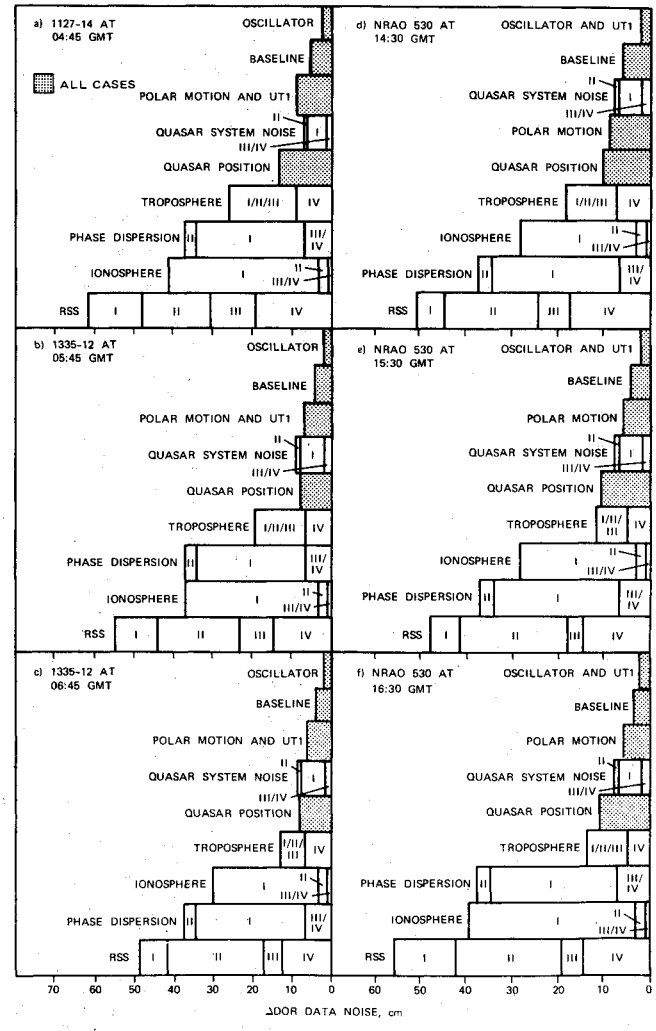

Fig. 8 Individual ΔDOR data noise contributors vs case number for the G/M and G/C baselines.

Antenna support is scheduled for CCE science tape recorder playback about every 8 h, or twice per orbit. Station passes 2–4 h long satisfy both recorder playback and radio metric data acquisition requirements. Operational experience indicates 2-h passes of Doppler and range from two different DSN complexes during a single orbit, updated weekly, easily maintains the necessary accuracy. The reference case uses data from the full Madrid and Canberra passes from orbit 315 (Fig. 1).

Both definitive and predictive orbit position uncertainties for a state-only strategy are evaluated using the navigation system error model and data sampling rates presented in Table 4. A 30-day mapping of these uncertainties identifies the major contributors to orbit accuracy decay.

Figure 9 compares the total position uncertainty with the individual contributions of data noise and the major modeling uncertainties. These data show that Doppler and range initially determine the apogee position to about 500 m and this uncertainty increases to about 3000 m after 30 days. The apogee position uncertainty has the following characteristics: 1) data noise dominates the early total uncertainty; 2) modeling errors overtake the data noise contribution near the middle of the prediction period; 3) the major contributor to modeling uncertainty early in the prediction period is the geopotential field; later solar pressure takes over; and 4) insufficient information content in two passes of Doppler and range in a single orbit prevents estimating either geopotential field or solar pressure parameters.

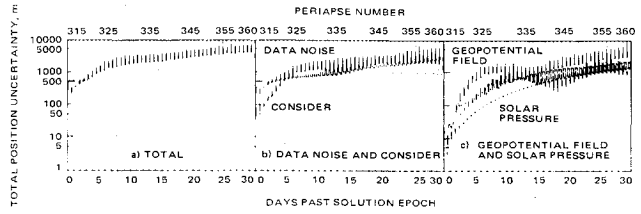

Fig. 9 Orbit position uncertainty using Doppler and range (Madrid and Canberra stations, see sampling rates in Table 4).

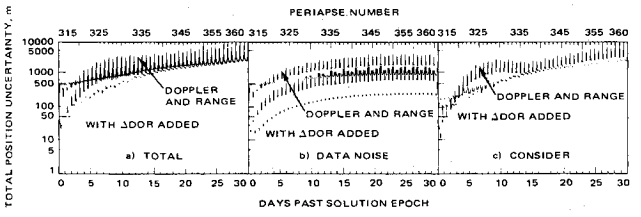

Fig. 10 Orbit position uncertainty improvement using case I ΔDOR with Doppler and range.

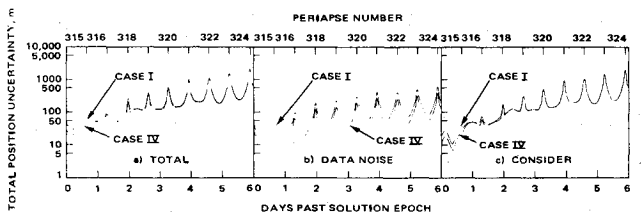

Fig. 11 Orbit accuracy comparison of cases I and IV ΔDOR data noise with Doppler and range.

Improvements with ΔDOR

Orbit accuracy improvements, possible when ΔDOR is added to Doppler and range, are now assessed. The performance capability is bounded using strategies with extremes of ΔDOR data noise, represented by cases I and IV summarized in Table 3.

When the six ΔDOR measurements from case I combine with the Doppler and range, initial apogee position uncertainty reduces from 500–25 m, as seen in Fig. 10a. This improvement results from reductions in both data noise and modeling errors. However, geopotential and solar pressure uncertainties cause modeling errors to propagate rapidly, equaling those of the reference case. The additional information content of ΔDOR measurements, while significantly lowering data noise, does not permit estimation of geopotential and solar pressure parameters necessary to improve orbit accuracy.

The capabilities of combining the six ΔDOR measurements from case IV with Doppler and range now are evaluated for comparison with the case I results. Figure 11 compares the data noise, modeling, and total errors for these two strategies. The modest improvement limits the comparison to the first six prediction days. The initial apogee position improves from 25 to 15 m, but the improvement is brief, as indicated by comparison of total errors in Fig. 11a. At first the modeling error component is smaller than the data noise, but the geopotential and solar pressure influences take over so that the total error for the two cases equalize after just three days.

Conclusions

This study identifies techniques for acquiring delta differential one-way range to determine Earth satellites in highly elliptical orbits. These techniques have been illustrated using the orbit of the Charged Composition Explorer spacecraft of the Active Magnetospheric Particle Tracer Explorers mission. Considerable parallax and rapidly changing viewing geometry degrade differential measurement accuracy, so acquisition strategies seek to minimize measurement noise. An S-band transmission capability and a small bandwidth further limit achievable measurement accuracy.

Significant ionosphere, troposphere, and phase dispersion contributions to total measurement noise remain after minimizing geometric influences. Predicted measurement noise reduces by a factor of four, using a water vapor radiometer ground instrument, dual frequency calibration, and a Galileo-like 38-MHz wideband transponder.

Coherent Doppler and range data were used to establish a reference case for comparison with capabilities of delta differential one-way range. This case is based on a state-only, two-station, single-orbit solution similar to strategies presently used for CCE operational orbit determination. Combining uncalibrated differential measurements with Doppler and range reduces the predicted one-sigma apogee uncertainty from 500 to 25 m. Additional improvement to 15 m results using calibrated measurements.

Calibration procedures reduce predicted measurement noise, but do not offer much improvement in orbit accuracy. Modeling uncertainties in the geopotential field and solar pressure limit predicted orbit accuracy much more than data noise. The measurement information content does not permit improved estimates of these parameters during the orbit determination process.

Accuracy improvements achieved with calibrated measurements offer far more benefit when acquiring differential measurements ever few days. A 16-h orbit, rather than the present 15:40 one, makes this possible with ground station viewing repeating every two days while the spacecraft completes three orbits. Adjusting the period with an on-board maneuver system to synchronize with desired baseline view periods, followed by occassional trims, provides frequent acquisition opportunities necessary to maintain orbit accuracy at the 15-m level.

This study examined use of baselines formed by the three Deep Space Network complexes, and none form orthogonal pairs. Additional baselines could increase the number of acquisition opportunities and offer better geometry. For example, adding stations in Chile, Japan, and South Africa forms several orthogonal baselines. Data acquired simultaneously across the view periods of two orthogonal baselines yield a series of instantaneous angular positions, offering an opportunity to greatly improve the orbit determination accuracy. More frequent viewing reduces the prediction interval and the need for high-precision gravity harmonic and solar pressure models.

The nominal acquisition strategy presented in this paper enhances the capabilities of Doppler and range. Validating these conclusions is best accomplished by a flight demonstration. However, the motivation for a demonstration arises from the need for increased orbit accuracy as compared to present requirements. Currently, spacecraft in highly elliptical Earth orbits conduct environmental studies that require modest position accuracies dictated by antenna pointing predictions more than by scientific objectives. These spacecraft will continue to be successfully supported with coherent Doppler and range until scientific goals require greater accuracy.

Missions planned for the early 1990's include several spacecraft having highly elliptical orbits, including those of the International Solar Terrestial Physics program, and a proposed orbiting radio telescope, QUASAT.[14] Navigation studies for these missions may show that the ΔDOR acquisition techniques introduced here can be effectively applied to improve orbit accuracies while also reducing antenna support requirements.

Acknowledgments

The research described in this paper was conducted at the Jet Propulsion Laboratory, California Institute of Technology, under contract with the National Aeronautics and Space Administration. Special appreciation is expressed to J. S. Border for generously sharing his valuable experience on numerous occasions. I am also thankful to V. N. Legerton for the timely implementation of software needed for this research.

References

[1]Melbourne, W.G. and Curkendall, D.W., "Radio Metric Direction Finding: A New Approach to Deep Space Navigation," AAS/AIAA Astrodynamics Specialist Conference, Jackson Hole, WY, Sept. 1977.

[2]Curkendall, D.W., "Radio Metric Technology for Deep Space Navigation: A Development Overview," AIAA Paper 78-1395, Aug. 1978.

[3]Christensen, C.S., Callahan, P.S., Moultrie, B., Donivan, F.F., and Wu, S.-C., "Results of a Demonstration of the Use of ΔVLBI Data for Precise Navigation of Interplanetary Spacecraft," AIAA Paper 80-1648, Aug. 1980.

[4]Border, J.S., Donivan, F.F., Finley, S.G., Hildebrand, C. E., Moultrie, B., and Skjerve, L.J., "Determining Spacecraft Angular Position with Delta VLBI: The Voyager Demonstration," AIAA Paper 82-1471, Aug. 1982.

[5]Taylor, T.H., Campbell, J.K., Jacobson, R.A. Moultrie, B., Nichols, R.A. Jr., and Riedel, J.E., "Performance of Differenced Range Data Types in Voyager Navigation," AIAA Paper 82-1473, Aug. 1982.

[6]Moultrie, B., Wolff, P.J., and Taylor, T.H., "The Performance of Differential VLBI Delay During Interplanetary Cruise," AIAA Paper 84-2048, Aug. 1984.

[7]Yunck, T.P. and Wu, S.-C., "Tracking Geosynchronous Satellites by Very-Long-Baseline Interferometry," *Journal of Guidance, Control and Dynamics*, Vol. 6, Sept.-Oct. 1983, pp. 382-386.

[8]Border, J.S., Donivan, F.F. Jr., Shiomi, T., and Kawano, N., "Precise Interferometric Tracking of the DSCS II Geosynchronous Orbiter," AIAA Paper 86-0402, Jan. 1986.

[9]Miller, J.K. and Nicholson, F.T., "Galileo Jupiter Approach Orbit Determination," *Journal of Astronautical Sciences*, Vol. 32, No. 1, Jan.-March 1984, pp. 63-80.

[10]Frauenholz, R.B. and Ellis, J., "Determining Highly Elliptical Earth Orbits with VLBI and ΔVLBI," *Journal of Astronautical Sciences*, Vol. 32, No. 2, April-June 1984, pp.. 159-174.

[11]Wu, S.-C., "Error Estimation for ΔVLBI Angle and Angle Rate Measurements Over Baselines Between a Ground Station and a Geosynchronous Orbiter," TDA Progress Rept. 42-71, Jet Propulsion Laboratory, California Institute of Technology, Pasadena, CA, July-Sept. 1982.

[12]Yuen, Joseph H., "Deep Space Telecommunications Systems Engineering," JPL Publication 82-76, Library of Congress Catalog Card 82-084114, July 1982.

[13]Thomas, J.B., Sovers, O.J., Fanselow, J.L., Cohen, E.J., Purcell, G.H. Jr., Rogstad, D.H., Skjerve, L.J., and Spitzmesser, D.J., "Radio Interferometric Determination of Source Positions, Intercontinental Baselines, and Earth Orientation with Deep Space Network Antennas—1971 to 1980," TDA Progress Rept. 42-73, Jet Propulsion Laboratory, California Institute of Technology, Pasadena, CA, Jan. March 1983.

[14]Jacobi, N., Christensen, C.S., and Hanna, M.C., "Study of Navigation Accuracy for the Proposed QUASAT Mission," AIAA Paper 85-0290, Jan. 1985.